



Published in final edited form as:

IEEE ASME Trans Mechatron. 2012 September 12; 18(1): 273–284. doi:10.1109/TMECH.2011.2163523.

Development and Evaluation of an Actuated MRI-Compatible Robotic System for MRI-Guided Prostate Intervention

Axel Krieger [Member, IEEE],

Department of Mechanical Engineering and the Laboratory for Computational Sensing and Robotics, Johns Hopkins University, Baltimore, Maryland, USA, and is presently with Sentinelle Medical Inc., Toronto, Canada.

Sang-Eun Song,

Laboratory for Computational Sensing and Robotics and the Department of Mechanical Engineering, Johns Hopkins University, Baltimore, Maryland, USA.

Nathan B. Cho,

Laboratory for Computational Sensing and Robotics and the Department of Mechanical Engineering, Johns Hopkins University, Baltimore, Maryland, USA.

Iulian Iordachita [Member, IEEE],

Laboratory for Computational Sensing and Robotics and the Department of Mechanical Engineering, Johns Hopkins University, Baltimore, Maryland, USA.

Peter Guion [Member, IEEE],

Radiation Oncology Branch, National Cancer Institute, National Institutes of Health, Bethesda, Maryland, USA.

Gabor Fichtinger [Member, IEEE], and

School of Computing, Queen's University, Kingston, Ontario, Canada.

Louis L. Whitcomb [Member, IEEE]

Laboratory for Computational Sensing and Robotics and the Department of Mechanical Engineering, Johns Hopkins University, Baltimore, Maryland, USA.

Abstract

This paper reports the design, development, and magnetic resonance imaging (MRI) compatibility evaluation of an actuated transrectal prostate robot for MRI-guided needle intervention in the prostate. The robot performs actuated needle MRI-guidance with the goals of providing (i) MRI compatibility, (ii) MRI-guided needle placement with accuracy sufficient for targeting clinically significant prostate cancer foci, (iii) reducing interventional procedure times (thus increasing patient comfort and reducing opportunity for needle targeting error due to patient motion), (iv) enabling real-time MRI monitoring of interventional procedures, and (v) reducing the opportunities for error that arise in manually actuated needle placement. The design of the robot, employing piezo-ceramic-motor actuated needle guide positioning and manual needle insertion, is reported. Results of a MRI compatibility study show no reduction of MRI signal-to-noise-ratio (SNR) with the motors disabled. Enabling the motors reduces the SNR by 80% without RF shielding, but SNR is only reduced by 40% to 60% with RF shielding. The addition of radio-frequency shielding is shown to significantly reduce image SNR degradation caused by the presence of the robotic device. An accuracy study of MRI-guided biopsy needle placements in a prostate phantom is reported. The study shows an average in-plane targeting error of 2.4 mm with

a maximum error of 3.7 mm. These data indicate the system's needle targeting accuracy is similar to that obtained with a previously reported manually actuated system, and is sufficient to reliably sample clinically significant prostate cancer foci under MRI-guidance.

Index Terms

Magnetic resonance imaging; robot manipulators; image-guided intervention; prostate cancer

I. Introduction

Prostate cancer is the most common cancer in men in the United States. In the United States in 2010, an estimated 217,730 men will be diagnosed with prostate cancer and 32,050 will die of this disease [2]. 1 in 6 U.S. men contract prostate cancer during their lifetime, and 1 in 36 U.S. men die of this disease. Approximately 1.2 million prostate biopsy procedures are performed annually in the U.S. [3], [4]. The two commonly used methods for screening men for prostate cancer are the prostate-specific antigen (PSA) blood test and the digital rectal exam (DRE). The American Cancer Society recommends screening men, beginning at age 50, yearly with PSA test and DRE. The present-day definitive diagnosis for prostate cancer is core needle biopsy, pursuant to either an elevated PSA level or a positive DRE. The "Gold Standard" of guiding biopsy, as well as of most local therapies, is transrectal ultrasound (TRUS) image guidance [5]. The physician manually places a TRUS probe in the rectum and, under ultrasound guidance, inserts a biopsy needle through the wall of the rectum into the prostate gland. The needle removes a half-cylinder of tissue, which is examined pathologically to determine if cancer is present. Several biopsy samples are taken from different areas of the prostate. Usually six (hence "sextant biopsy") to eighteen cores are removed from upper, mid, and lower areas of the left and right sides to obtain a representative sampling of the gland and determine the degree and extent of cancer.

Trus-guided prostate biopsy is widely employed due to its real-time nature, relatively low cost, and ease of use. Its limitations, however, are substantial. Although shortcomings have been known over a decade and often reconfirmed, there are no major improvements in sight. Using standard techniques, biopsy of men with PSA blood test values in the range of 4–10 ng/ml generally result in a cancer detection rate of 20%–30% [6], [7]. Numerous studies have shown that TRUS-guided prostate biopsy fails to detect cancer in at least 20% of patients with cancer [8]–[11]. Studies report that TRUS-guided biopsies are limited by low sensitivity of 60% with only 25% positive predictive value, in which no significant change has been seen, for example, by Terris et al. in the past 15 years [12]. Such observations have been corroborated by many, including [4], [13]–[16]. For example Gann et. al. report "Seventy to 80% of the approximately 1.2 million patients who undergo prostate biopsy each year in the United States receive negative results (i.e., no cancer) but cannot be completely reassured because a cancer may have been missed by [TRUS-guided biopsy] sampling error" [4]. Studies have shown that more than one-third of men whose first biopsies were negative were re-biopsied within the next 5 years, resulting in a large number of repeat biopsy cases [16]. Despite advances in ultrasound imaging methods, TRUS imaging is generally unable to differentiate between healthy tissue and cancerous lesions in the prostate. In consequence, contemporary TRUS-guided biopsy cannot identify or target lesions, and cancerous nodes of clinically significant size are routinely missed. Clearly, significantly improved alternatives to TRUS image guidance are needed.

This paper is organized as follows: This section reviews the need for magnetic resonance imaging (MRI) guided prostate intervention, Section II reports the system design, Section III

reports the results of a performance evaluation of the system, and Section IV summarizes the results of this study.

A. The Case for MRI-Guided Needle Intervention

MRI possesses many of the capabilities that TRUS is lacking. MRI is an attractive choice for image-guidance, primarily due to its high sensitivity for detecting prostate tumors [10], [17]–[20], high spatial resolution, excellent soft tissue contrast, and volumetric imaging capabilities.

Advances with phased array pelvic and endorectal coils have dramatically enhanced the ability of MRI to visualize prostate tissues [21], [22]. MRI can clearly visualize the prostate and its substructure including the peripheral zone (PZ). As the PZ is the most common site of origin of prostate cancer, localizing and targeting suspicious PZ lesions during prostate biopsy is expected to increase cancer detection rate. T2 weighted images can identify suspicious nodules in the prostate, allowing targeted biopsy and subsequent local therapy.

Several novel MRI methods are currently being developed in an effort to improve the specificity of prostate cancer detection and characterization, including MRI spectroscopy [10], [23], dynamic contrast enhancement, T2 maps, and diffusion imaging [24], [25]. MRI can visualize the distribution and buildup of injected liquid agents in the prostate [26], [27], and solid capsules [26], [28]. MRI can also monitor the progress of thermal therapies in real-time [29], [30].

In summary, MRI is a promising image guidance modality for prostate interventions. There is also an urgent clinical need to investigate diagnostic capabilities of emerging MR imaging techniques. MRI could potentially overcome the shortcomings of ultrasound as the image guidance modality for the diagnosis and local therapy of prostate cancer.

B. Challenges in MRI-Guided Needle Intervention

Recently a flurry of research activity in MRI-guided intervention has resulted in the development of several prototype robotic systems for MRI-guided needle-intervention in the prostate [18], [20], [31]–[33]. Most reported MRI-guided needle-intervention systems for closed-bore 1.5 T and 3.0 T MRI scanners (e.g. for prostate, breast, and other applications) do not permit needle insertions to be performed while the patient is inside the MRI scanner bore. Most previously reported MRI-guided prostate intervention robots, reviewed in Section I-D, require the patient to be removed from the scanner during the interventional procedure, e.g. needle insertion, biopsy, or fiducial marker placement. In all previously reported *clinical* prostate systems, if a confirmation image of a needle placement is required, the patient must again be returned to the scanner for imaging. Repeated motion of the patient in and out of the scanner bore decreases needle placement accuracy in consequence of patient motion, complicates confirmation imaging, precludes the use of real-time MR imaging during an intervention, and significantly increases procedure time.

C. The APT-III System for MRI-Guided Transrectal Needle Intervention in the Prostate

This paper reports the development of the APT MRI III robot, a compact prototype of an actuated robot designed to enable transrectal MRI-guided needle access of the prostate (Figures 1 and 2). The name APT MRI is an acronym for *Access to Prostate Tissue under MRI Guidance*. The robot performs actuated needle MRI-guidance with the goals of providing (i) MRI compatibility, (ii) MRI-guided needle placement with accuracy sufficient for targeting clinically significant prostate cancer foci, (iii) reducing interventional procedure times (thus increasing patient comfort and reducing opportunity for needle targeting error due to patient motion), (iv) enabling real-time MRI monitoring of

interventional procedures, and (v) reducing the opportunities for error that arise in manually actuated needle placement. This present paper reports results relevant to the first two goals. Accomplishment and quantitative evaluation of the final three goals will require additional engineering development and Phase II clinical trials are beyond the scope of this paper, and are the goal of our future work. The design of the robot, employing two degree-of-freedom (2-DOF) piezo-ceramic-motor actuated needle guide positioning and manual needle insertion, is reported. The purpose of this prototype is to develop and validate experimentally the technologies (mechanical, electrical, and software) necessary for the future development of a fully-actuated, clinically qualified robotic device capable of supporting in-bore MRI-guided needle intervention of the prostate including (a) biopsy, (b) injection, (c) fiducial marker insertion, and (d) focal therapy.

The new APT MRI III robot builds upon our previous development of a family of manually-actuated MRI-guided system, the APT-I and APT-II, for MRI-guided transrectal needle placement in the prostate. The principal advances of the APT-II over the APT-I are (i) novel manipulator mechanics employing a steerable needle guide and (ii) a novel six degree of freedom hybrid tracking method, comprised of passive fiducial tracking for initial registration and subsequent incremental motion measurements. The APT-I, in contrast, employed custom MRI tracking sequences and custom tracking calibration for each individual scanner. The APT-II hybrid tracking system, using only standard MRI sequences, allows it to be easily used on different MRI scanners.

The APT-I and APT-II systems have been used initially in canine studies, [26], [27], [34], [35], and subsequently in clinical studies at three different clinical sites: (i) the National Institutes of Health (NIH) National Cancer Institute (NCI) Bethesda, Maryland, (ii) the Radiation Oncology Department at Princess Margaret Hospital (PMH), Toronto, Canada, and (iii) the Johns Hopkins University (JHU) Department of Radiology, Baltimore, Maryland. Each clinical site uses a different MRI scanner, different diagnostic prostate imaging sequences, and different clinical protocols separately approved by the local institution's Institutional Review Board (IRB). To date, the APT-I system was employed in 37 clinical procedures at NIH [36]–[38], and the APT-II system has been employed in 20 clinical human-subject trials at NIH, PMH, and JHU, for a total of 57 clinical procedures to date [39]–[41]. Clinical studies using the APT-II are ongoing at NIH, PMH, and JHU.

D. Previously Reported MRI-Compatible Prostate Intervention Systems

This section reviews previously reported MRI-compatible systems for prostate intervention utilizing transrectal, transperineal, and transluteal approach.

1. *Transrectal Approach:* In [26], [27], [34]–[36], [38], [42] we reported the development and clinical evaluation of two generations of MRI-guided system for transrectal prostate biopsies, therapy injection, and marker placements. The APT-I and APT-II systems incorporate a single-loop MRI endorectal imaging coil and employ active or passive tracking, respectively, for device localization. These clinical prototypes have been successfully used in 57 clinical human subject clinical procedures to date. To the best of our knowledge, the APT-I and APT-II systems are the only clinically utilized systems for transrectal MRI-guided access to the prostate employing active or hybrid tracking.

In [43] Beyersdorff and in [44] Engelhard report MRI-guided transrectal needle biopsies in clinical studies with a system (InVivo Germany GmbH, Schwerin, Germany) employing manual alignment and passive tracking of a needle sleeve. In [45] Barentsz reports phantom studies with a MRI-compatible pneumatically actuated transrectal robot. Elhawary reported phantom experiments with a

prototype robotic system using linear piezo-ceramic motors for transrectal prostate biopsy [46].

2. *Transperineal Approach:* MRI-guided transperineal prostate intervention has been demonstrated in clinical studies inside an open MRI scanner [47] and conventional closed MRI scanner with the use of static needle-guiding templates [48]. A surgical assistant robot reported by Chinzei [49] was adapted to assist transperineal intra-prostatic needle placement [50]. Tadakuma reported the use of dielectric elastomer actuators in a pre-clinical prototype MRI-compatible robot for transperineal needle placement in the prostate [51], [52]. Stoianovici reported phantom experiments with a pneumatically actuated device for transperineal brachytherapy seed placement [53]. In [54] and [55] we reported the development of a device with a pneumatically actuated needle guide and manual needle insertion for transperineal needle placement in the prostate, and reported phantom experiments. Goldenberg reported phantom studies and MRI compatibility tests with a robotic system employing ultrasonic actuators in closed MRI scanners [56]. In [57] van den Bosch reported a hydraulically and pneumatically actuated tapping robot.
3. *Transgluteal Approach:* Zangos reported preliminary clinical results with 25 patients using the transgluteal approach with an open configuration 0.2 T MRI scanner, with targeting based on T1 and T2 diagnostic images previously acquired with a 1.5 T scanner [58]. However, they did not detail the technique used for the fusion of high-field diagnostic and low-field intra-operative MRI sequences. Zangos and Vogl reported usage of the Innomotion pneumatic robot in a cadaver study at 1.5 T for transgluteal prostate needle placements [59], and transgluteal MRI-guided galvanotherapy [60].

E. Clinically Significant Prostate Cancer Tumor Size

Prostate cancer is a progressive disease. As tumor volume increases, so does malignant potential. McNeal *et al.* found that metastasis occurs only in prostate cancer tumors larger than 4 ml and with Gleason Grades¹ of 4 or 5 [62]. Some authors report tumor volume to be the single most important factor in predicting cancer progression [63], [64]. A 0.5 ml prostate cancer volume has been proposed as the limit of clinically significant prostate cancer foci volume [65]. Several studies report that small-volume prostate cancers (0.5 ml or less) with Gleason grades below 4 are not clinically significant [13], [66], [67]. MRI with endorectal imaging coil with 1.5 T field strength currently possesses the ability to reliably detect prostate cancer with foci volume greater than 1 ml [68]. Increased field strength of clinically available scanners (i.e. from 1.5 T to 3.0 T) and newly developed MR imaging methods might reduce the detectable prostate cancer foci volume to the clinically relevant volume of 0.5 ml. Assuming spherical shaped tumors, a 1 ml tumor volume corresponds to a sphere with diameter 12.4 mm. A 0.5 ml tumor volume corresponds to a sphere with diameter 9.8 mm. We conclude that an MRI guided biopsy system employing a targeting accuracy of 5 mm or better (about half the minimum size of clinically relevant prostate cancer foci) could reliably access under MRI guidance clinically significant prostate cancer foci.

II. APT-III Robot System Design

This Section reports the design of a robot for transrectal prostate interventions with actuated needle alignment and manual needle insertion. Figure 1 shows a CAD model of the robot

¹The Gleason Grade is a widely used system for grading cell differentiation (cancer severity) in prostate cancer tissue samples. A score of 1 indicates a least aggressive cancer, and a score of 5 indicates a highly aggressive cancer likely to metastasize [61].

and position of both the robot and patient in the MRI scanner. Figure 2 shows a close-up photograph of the APT-III actuated robot. The robot employs manipulator kinematics similar to the APT-II system [41], [42]. The APT-III employs the rectal sheath, steerable needle guide, and passive 6-DOF positioning arm designed originally for the APT-II; all other parts of the APT-III are newly designed specifically for the APT-III. The robot provides actuated needle guidance. Needle insertion is performed manually in the prototype reported herein. This prototype is thus a stepping-stone towards a next-generation design that incorporate actuated needle insertion.

The robot consists of a rotation stage and a translation stage with flexible coupling, integrated in a motor housing. The rotation and translation stages actuate 2-DOF angulation of the needle guide. Non-magnetic piezo-ceramic motors from the HR series piezo-electric motors (Nanomotion Inc., Yokneam, Israel) were selected for actuation [69]. Motors are placed 20 cm or more away from the prostate to eliminate susceptibility artifacts on the MR images caused by metallic motor components. Nanomotion non-magnetic HR motors consist of one, two, four, or eight linear piezo-ceramic elements stacked inside an aluminum enclosure. The motors are not back-drivable.

A. Rotation Stage

The rotation stage controls the axial rotation of the entire transrectal probe assembly including the steerable needle guide. Figure 3 shows a CAD model of the rotation stage for the robot. Nanomotion motors can be mounted either radially or axially to exert rotation of a ceramic drive ring. The rotation axis is generally aligned with the main axis of the MRI scanner bore. Radial space is limited in a MRI scanner bore, while axial space is ample. Hence, axial motor configuration was selected for the rotation stage. Single-element motors (HR-1 motors) were selected for the rotation stage, since they are best suited for axial configuration in combination with a small drive ring. Each HR-1 motor provides a dynamic stall force of 4 N and exerts a pre-load of 18 N on the ceramic drive surface. The pre-load is applied constantly and provides high static friction force. Aligning the HR-1 motors in opposing pairs limits the net force exerted on the ring and minimizes deflection and bearing loads of the rotation stage. Maximum velocity for the HR series motors is 250 mm/sec.

Experience with the APT-II system showed that manually turning a medium sized knob provided sufficient torque for the rotation of the rectal sheath. Applying higher torques above human capabilities could potentially cause injuries for patients. Hence, the requirements for the rotational torque were based on human factors. Data reported in [70] indicates mean maximum hand turning strengths of adult males when turning a knurled knob of diameter of 1.5 inches to be 1.03 Nm. This knob size is only slightly smaller as the 2-inch rotation knob of the APT-II system. Torque requirements for the rotation stage were thus set at 1 Nm

Three pairs of non-back-drivable HR-1 motors, with a combined dynamic stall force of 24 N for the six motors, provide a designed maximum torque of 1.08 Nm, when rotating a drive ring with center diameter of 90 mm. The combination of three pairs of HR-1 motors, spaced evenly in 120 degrees increments along the circumference of a 90-mm-diameter drive ring, meets the torque requirements and was selected for the robot.

B. Translation Stage

The translation stage controls the tilt angle of the steerable needle guide within the transrectal probe. Figure 4 shows a CAD model of the translation stage for the actuated robot using two Nanomotion HR-4 motors with four motor elements each. A MRI-compatible implementation of crossed roller bearings is difficult to design and would be

expensive. Our initial mechanical evaluation of a piezo-electric motor and linear-bearing test assembly revealed that better motor performance can be achieved when linear bearings are eliminated, and side-to-side alignment of the drive shaft is set using only the fingers of opposing motors. This low-cost linear drive implementation was used for the translation stage of the actuated robot.

Opposing pairs of HR-4 Nanomotion motors are axially preloaded on ceramic drive strips and provide linear motion of a drive shaft that slides axially forward and backward on a motor plate. Side-to-side alignment of the drive shaft is set by the pre-load of the opposing ceramic motor fingers. The low-cost bearing implementation reduces the dynamic stall force and reduces the maximum speed. A needle tilt angle range of 17.5° to 40° was selected, based upon data obtained with the APT-I, to ensure needle access to the entire prostate. The linear travel necessary for a needle tilt angle range of 17.5° – 40° is 28.7 mm. Only device friction has to be overcome to change the needle angle and slow speeds are acceptable for actuating the needle angle change. The short travel, slow speed requirements, combined with closed-loop position control allow the usage of the non-back-drivable HR-4 motors in combination with the low-cost bearing implementation.

C. Materials

The robot is constructed mostly of plastic materials, foremost of Ultem[®] (Polyetherimide), (SABIC Inc., Pittsfield, MA, USA), selected for its structural stability, machinability, and low cost. Ball bearings and bearing races for the rotation stage are fabricated of Zirconium Oxide (VXB Inc., Anaheim, CA, USA). Vertical stops and rotating parts of the flexible coupling for the translation stage are constructed of Teflon[®], (Dupont, Wilmington, DE, USA), to reduce friction. All larger metallic components are placed inside the motor housing, such as motors and motor plates. The motor plates for the rotation stage and translation stage are constructed of aluminum for increased stability and heat dissipation, in comparison to Ultem[®]. The motor housing is separated by 20 cm from the field-of-view (FOV) by the rotation shaft and rectal sheath to avoid creation of susceptibility artifacts on MR images. The rectal sheath is machined from USP-VI medical grade Ultem[®] with small aluminum and brass parts for needle guide and axles.

D. Position Tracking

The robot uses the hybrid tracking method described in [42]. Initial device registration is performed using two Beekley markers (Beekley Inc., Bristol, CT, USA) integrated into the rectal sheath and two markers placed coaxially to the needle guide. The initial position and orientation of the robot is computed after automatic segmentation of the markers on MR images. The robot employs electro-optical encoding for the needle rotation and needle tilt angle.

The advantage of fiber optic joint encoding over electrooptical joint encoding, is the inherent MRI safety and compatibility of fiber optics [42]. Advantages of electro-optical encoders include the ubiquitous availability of inexpensive commercial electro-optical encoders, high resolution and repeatability, and easy encoder signal integration into a controller. In contrast to the system reported in [42], the actuated robot already contains piezoelectric motors, which require power connections. Adding cables for supplying the electrooptical encoders with power and conducting encoder signals does not significantly add to the complexity of the design or the safety risk.

Modular EM1 electro-optical encoders (US Digital, Vancouver, BC, Canada), code wheel, and code strip were selected for joint encoding. Encoding resolution for rotation is $(360^\circ/10000 \text{ counts}) = 0.036^\circ/\text{count}$. The resolution for encoding translation is 25.4 mm/2000

counts = 0.013 mm/count. The calculated average needle angle resolution is thus $((40^\circ - 17.5^\circ)/28.7 \text{ mm}) \cdot (0.013 \text{ mm/counts}) = 0.01^\circ/\text{count}$. This resolution is an order of magnitude better than that of the fiber optical encoders of the APT-II system reported in [42], [71], which achieved $0.25^\circ/\text{count}$ resolution for rotation and $0.1^\circ/\text{count}$ resolution for needle tilt angle.

E. Passive 6-DOF Mounting Arm

The APT-III is designed to be mounted on the passive adjustable 6-DOF mounting arm originally developed for the APT-I and APT-II. The mounting arm consists of two parts: a slide and rail assembly (Igus Inc., E. Province, RI, USA) for linear motion parallel to the scanner bore with an integrated locking mechanism and a custom designed passive arm. The passive arm is comprised of a rigid plastic rod connected with spherical joints to the slide and to the manipulator, respectively. A locking mechanism is built into the rod to simultaneously immobilize both joints, once the manipulator is placed at its desired location. The passive arm is designed to resist at a force of up to 30 N applied at 200 mm from its distal joint with a maximum deflection of 1 mm. The 30 N force limit was chosen based on our previous clinical experience to avoid harm to the patient. The 1 mm deflection limit was chosen because it is significantly smaller than the typical minimum MRI slice thickness of 2–3 mm.

F. Controller

The controller box contains two Nanomotion AB5 motor amplifiers, a DMC-21x3 Ethernet motion controller (Galil Motion Control, Rocklin, CA, USA), and a EIR-M-ST fiber optic to Ethernet media converter (B&B Electronics Mfg. Co., Ottawa, IL, USA). The only electrical connection to the controller is a filtered 24 V DC power supply through the penetration panel. External communication is via fiber optic Ethernet. IP66/67 Harsh Environment Multimode Duplex LC Cable (L-com Inc., North Andover, MA, USA) was selected for the fiber optical connection because of its rugged design. The controller box was located inside the MRI scanner room near the control room wall waveguide that allows passage of electrical and fiber-optic cables. The controller box was located outside the 5 G (0.5 mT) boundary where regular surgical instruments can be used.

G. Radio-Frequency Shielding

The controller box aluminum shell is grounded to earth ground. The cable connecting the robot to the controller is shielded with radio-frequency (RF) shielding (Z-3250-CN High Performance EMI Shielding Cloth, Zippertubing Co., Los Angeles, CA, USA). The cable shield is connected to ground via the controller box aluminum shell. We tested two different shielding configurations for the APT-III robot: (a) unshielded as shown in Figure 7 (left image) and (b) shielded with Z-3250-CN radio-frequency (RF) shielding cloth as shown in Figure 7 (right image). In the latter case the APT-III shield was connected to ground via the cable shield.

III. APT-III Needle Targeting and MRI-Compatibility Evaluation

This Section reports the results of MRI compatibility phantom studies with the APT MRI III, in order to determine (a) the accuracy of MRI-guided needle placement and (b) the effects of the robot on signal-to-noise-ratio (SNR) of the MR images. All tests were performed on a 3 T Philips Achieva MRI scanner (Philips Medical Systems, Best, NL).

A. MRI-Guided Needle Targeting Accuracy Study

The targeting accuracy of the actuated transrectal prostate robot was evaluated in a phantom study. The actuated robot was secured on top of a cushion on the MRI scanner table. The

rectal sheath of the robot was placed inside a prostate phantom (CIRS Inc, Norfolk, VA, USA). Seven targets were selected at clinically relevant locations in the prostate gland, from base to mid gland to apex, on T2 weighted axial TSE images (Figure 6, first row). For each target, our APT software calculated the necessary needle angles and insertion depth values for correct needle placement. Rotation and needle angle parameters were exported to the motor controller software, the robot was moved, and the needle guide was aligned with the target. The insertion of the biopsy needle was performed manually to the depth specified by the APT software.

The location of the needle was confirmed in axial TSE proton density images that showed the void created by the biopsy needle tip close to the target point (Figure 6, second row). The in-plane error for each of the seven biopsies, defined as the distance of the target to the biopsy needle line was subsequently calculated to assess the accuracy of the robot. The average in-plane error was 2.4 mm with a maximum error of 3.7 mm. This needle placement accuracy is similar that reported in a study of 81 *in-vivo* needle biopsies with the APT-I and APT-II systems, where a needle targeting error of range of 0.1 to 6.5 mm with a mean of 2.3 mm and a standard deviation of 1.3 mm were measured [72]. This MRI-guided needle placement accuracy is sufficient to target clinically significant prostate cancer foci (Section I–E) which are presently understood to be tumors of diameter 9.8 mm or larger [13], [65]–[67].

For better evaluation of the targeting accuracy every biopsy needle placement in the prostate phantom was followed by the placement of a glass needle to the same depth. The void created by the glass needle is artifact-free and concentric to the needle, in contrast to the metallic biopsy needle. The location of the glass needle was confirmed in axial TSE proton density images (Figure 6, third row). The average in-plane error for the glass needles was 1.9 mm with a maximum error of 3.1 mm. Analyzing the error reveals an average shift between glass needle void location and biopsy needle void location of 0.5 mm in the A–P direction, corresponding to the direction of the frequency encoding gradient — corroborating other studies of needle artifact localization in 3T MR images [73].

The push rod of the prototype actuated robot, controlling the needle tilt angle, came loose a few times during the study, possibly contributing to the targeting error. The unstable position of the actuated robot on top of a cushion may have increased the targeting error as well.

B. MRI Signal-to-Noise Ratio Study

SNR is the ratio of signal intensity in the region-of-interest (ROI) to the intensity of noise intensity in the periphery. We employ the National Electrical Manufacturers Association (NEMA) standard for determining SNR in MRI [74]. Signal intensity is defined as the mean pixel intensity in the ROI. Noise intensity is defined as the root mean square (RMS) signal intensity outside of the tissue or phantom. Each set of experiments consisted of a saline phantom being imaged alone (baseline) and subsequently imaged in the presence of each actuator in its power-off configuration, power-on configuration, and moving configuration. The receiving imaging coils used for the experiments were two-channel medium-size flex coils consisting of two panels. One panel was placed underneath the phantom, while the other one was placed on top of the phantom (Figure 7). We chose this coil and phantom setup because, in earlier trials with the APT-I and APT-II systems, it provided image quality comparable to that observed in clinical prostate imaging on the same scanner.

Three commonly used MRI sequences for diagnostic and functional imaging were selected to test the compatibility of the actuators (Table I): T1-weight Fast Field gradient Echo (T1-FFE) and T2-weight Turbo Spin Echo (T2-TSE) sequences representative of diagnostic

imaging, and Turbo Field Echo (TFE) sequences representing real-time imaging used for functional imaging. The phantom was imaged under the eleven configurations given in Table II.

In configurations 1, 2, 4, 6, 8, and 10 the body of the robot was unshielded. In configurations 3, 5, 7, 9, and 11 the body of the robot was covered with additional radio-frequency (RF) shielding. In configurations 4–10 the electro-optical joint encoders were energized. Ten image slices were obtained of the phantom for each configuration for each image sequence and the SNR was calculated for each image slice. Figure 8 shows the SNR results, averaged for the 10 slices, for each of the three sequences. Figure 9 shows representative T2 weighted images of the saline phantom under different configurations acquired during the MRI compatibility study.

The following are the most significant observations of the MRI compatibility study for the actuated robot:

1. The SNR exhibits modest spatial variation – measurements were uniform across the multiple scan slices.
2. The actuated robot does not cause any measurable reduction in SNR in the motors-off configuration (col. 2 and 3 of Figure 8) – thus enabling interleaved imaging and motion. Note that the motors are not back-drivable.
3. Turning the controller on with motors disabled (col. 4 and 5 of Figure 8) reduces the SNR by 50% in without RF shielding, but SNR is only slightly degraded with RF shielding.
4. Turning the controller on with motors enabled (col. 6 through 11 of Figure 8) reduces the SNR by 80% without RF shielding, but SNR is only reduced by 40% to 60% with RF shielding.
5. Noise appears as vertical “zipper” streaks in the MR images (Figure 9) - a well-known effect of RF interference.
6. All three MR scan sequences (T1, T2, and TFE) show similar SNR behavior.
7. The addition of RF shielding improves the SNR by a factor 200% to 500% in comparison to the same robot without RF shielding (col. 6–11 of Figure 8).

The SNR degradation observed for the motors-on case is not a problem in practice because the patient and the needle are both normally motionless during most MRI scanning sequences — to avoid MRI motion artifacts. These data indicate that the motors can be disabled or turned off during MRI scans, and will thus cause no measurable SNR degradation.

IV. Conclusion

This paper reported the design, development, MRI compatibility evaluation, and MRI-guided targeting evaluation of an actuated transrectal prostate robot for MRI-guided intervention. The robot is a technological step towards the goal of a fully-actuated robotic device capable of in-bore MRI-guided needle interventions of (a) biopsy, (b) injection, and (c) fiducial marker insertion. The present version of the robot reported herein employs actuated needle guide positioning and manual needle insertion. Piezo-ceramic motors were selected as actuators for the robot.

Phantom targeting experiments demonstrated the feasibility of using the robot for MRI-guided prostatic needle procedures. A needle targeting accuracy study of seven MRI-guided

biopsy needle placements in a prostate phantom exhibited average in-plane error for the biopsy needles was 2.4 mm with a maximum error of 3.7 mm. These data indicate the system's needle targeting accuracy is sufficient to reliably sample clinically significant prostate cancer foci under MRI-guidance.

The MRI compatibility of the robot was analyzed, showing no measurable reduction of SNR in the motor-off configuration and a 40% to 60% reduction in SNR with the motors on. The addition of RF shielding significantly improved SNR quality. The SNR degradation observed for the motors-on case is not a problem in practice because the patient and the needle are both normally motionless during most MRI scanning sequences (to avoid motion artifacts). These data indicate that the motors can be disabled or turned off during MRI scans, and will thus cause little or no SNR degradation.

In future work we propose to develop a clinically qualified version of the APT-III incorporating a fully actuated needle insertion module, improved MRI-compatible power electronics, e.g. [75], and improved mechanical design.

Acknowledgments

We are grateful to Mr. Mike Franckowiak and Mr. Walter Krug for their expert machining of the actuated robot prototype.

This study was supported by the National Institutes of Health under Grant RO1-EB02963. Gabor Fichtinger was funded as Cancer Care Ontario Research Chair. The Johns Hopkins University has licensed some of the intellectual property employed in the device and system described herein to Sentinelle Medical Inc., Toronto, Canada.

REFERENCES

1. Krieger, A.; Iordachita, I.; Song, S-E.; Cho, NB.; Guion, P.; Fichtinger, G.; Whitcomb, LL. Development and preliminary evaluation of an actuated MRI-compatible robotic device for MRI-guided prostate intervention. Proc. IEEE Int Robotics and Automation (ICRA) Conf; 2010. p. 1066-1073.
2. American Cancer Society. Cancer Facts and Figures 2010. Atlanta: American Cancer Society; 2010.
3. Haker S, Mulkern R, Roebuck J, Barnes A, DiMaio S, Hata N, Tempny C. Magnetic resonance-guided prostate interventions. Topics in Magnetic Resonance Imaging. 2005; vol. 16(no. 5):355. [PubMed: 16924169]
4. Gann P, Fought A, Deaton R, Catalona W, Vonesh E. Risk factors for prostate cancer detection after a negative biopsy: A novel multivariable longitudinal approach. Journal of Clinical Oncology. 2010; vol. 28(no. 10):1714. [PubMed: 20177031]
5. Presti JC. Prostate cancer: assessment of risk using digital rectal examination, tumor grade, prostate-specific antigen, and systematic biopsy. Radiologic Clinics of North America. 2000 Jan; vol. 38(no. 1):49–58. [PubMed: 10664666]
6. Terris MK, Wallen EM, Stamey TA. Comparison of mid-lobe versus lateral systematic sextant biopsies in the detection of prostate cancer. Urologia Internationalis. 1997; vol. 59(no. 4):239–242. [PubMed: 9444742]
7. Roehl KA, Antenor JAV, Catalona WJ. Serial biopsy results in prostate cancer screening study. Journal of Urology. 2002 Jun; vol. 167(no. 6):2435–2439. [PubMed: 11992052]
8. Norberg M, Egevad L, Holmberg L, Sparén P, Norlén BJ, Busch C. The sextant protocol for ultrasound-guided core biopsies of the prostate underestimates the presence of cancer. Urology. 1997 Oct; vol. 50(no. 4):562–566. [Online]. Available: [http://dx.doi.org/10.1016/S0090-4295\(97\)00306-3](http://dx.doi.org/10.1016/S0090-4295(97)00306-3). [PubMed: 9338732]
9. Rabbani F, Stroumbakis N, Kava BR, Cookson MS, Fair WR. Incidence and clinical significance of false-negative sextant prostate biopsies. Journal of Urology. 1998 Apr; vol. 159(no. 4):1247–1250. [PubMed: 9507846]

10. Wefer AE, Hricak H, Vigneron DB, Coakley FV, Lu Y, Wefer J, Mueller-Lisse U, Carroll PR, Kurhanewicz J. Sextant localization of prostate cancer: comparison of sextant biopsy, magnetic resonance imaging and magnetic resonance spectroscopic imaging with step section histology. *Journal of Urology*. 2000 Aug; vol. 164(no. 2):400–404. [PubMed: 10893595]
11. Taira AV, Merrick GS, Galbreath RW, Andreini H, Taubenslag W, Curtis R, Butler WM, Adamovich E, Wallner KE. Performance of transperineal template-guided mapping biopsy in detecting prostate cancer in the initial and repeat biopsy setting. *Prostate Cancer Prostatic Dis*. 2010 Mar; vol. 13(no. 1):71–77. [Online]. Available: <http://dx.doi.org/10.1038/pcan.2009.42>. [PubMed: 19786982]
12. Terris MK. Strategies for repeat prostate biopsies. *Curr Urol Rep*. 2009 May; vol. 10(no. 3):172–178. [PubMed: 19371473]
13. Bak JB, Landas SK, Haas GP. Characterization of prostate cancer missed by sextant biopsy. *Clinical Prostate Cancer*. 2003 Sep; vol. 2(no. 2):115–118. [PubMed: 15040873]
14. Goossen T, Wijkstra H. Transrectal ultrasound imaging and prostate cancer. *Arch Ital Urol Androl*. 2003 Mar; vol. 75(no. 1):68–74. [PubMed: 12741351]
15. Djavan B, Margreiter M. Biopsy standards for detection of prostate cancer. *World J Urol*. 2007 Mar; vol. 25(no. 1):11–17. [Online]. Available: <http://dx.doi.org/10.1007/s00345-007-0151-1>. [PubMed: 17342490]
16. Welch H, Fisher E, Gottlieb D, Barry M. Detection of Prostate Cancer via Biopsy in the Medicare–SEER Population During the PSA Era. *Journal of the National Cancer Institute*. 2007; vol. 99(no. 18):1395. [PubMed: 17848671]
17. Yu KK, Hricak H. Imaging prostate cancer. *Radiologic Clinics of North America*. 2000 Jan; vol. 38(no. 1):59–85. viii. [PubMed: 10664667]
18. Pondman KM, Ftterer JJ, ten Haken B, Kool LJS, Witjes JA, Hambroek T, Macura KJ, Barentsz JO. MR-guided biopsy of the prostate: an overview of techniques and a systematic review. *Eur Urol*. 2008 Sep; vol. 54(no. 3):517–527. [Online]. Available: <http://dx.doi.org/10.1016/j.eururo.2008.06.001>. [PubMed: 18571309]
19. Ftterer JJ, Barentsz J, Heijmijnk ST. Imaging modalities for prostate cancer. *Expert Rev Anticancer Ther*. 2009 Jul; vol. 9(no. 7):923–937. [Online]. Available: <http://dx.doi.org/10.1586/era.09.63>.
20. Elhawary H, Tse ZTH, Hamed A, Rea M, Davies BL, Lamperth MU. The case for MR-compatible robotics: a review of the state of the art. *International Journal of Medical Robotics and Computer Assisted Surgery*. 2008 Jun; vol. 4(no. 2):105–113. [Online]. Available: <http://dx.doi.org/10.1002/rcs.192>. [PubMed: 18481822]
21. Adusumilli S, Pretorius ES. Magnetic resonance imaging of prostate cancer. *Seminars in Urologic Oncology*. 2002 Aug; vol. 20(no. 3):192–210. [PubMed: 12215973]
22. Quick HH, Serfaty JM, Pannu HK, Genadry R, Yeung CJ, Atalar E. Endourethral MRI. *Magnetic Resonance in Medicine*. 2001 Jan; vol. 45(no. 1):138–146. [PubMed: 11146495]
23. Ménard C, Smith IC, Somorjai RL, Leboldus L, Patel R, Littman C, Robertson SJ, Bezabeh T. Magnetic resonance spectroscopy of the malignant prostate gland after radiotherapy: a histopathologic study of diagnostic validity. *International Journal of Radiation Oncology Biology Physics*. 2001 Jun; vol. 50(no. 2):317–323.
24. Chan I, Wells W, Mulkern RV, Haker S, Zhang J, Zou KH, Maier SE, Tempany CMC. Detection of prostate cancer by integration of line-scan diffusion, T2-mapping and T2-weighted magnetic resonance imaging, a multichannel statistical classifier. *Medical Physics*. 2003 Sep; vol. 30(no. 9):2390–2398. [PubMed: 14528961]
25. Westin C-F, Maier SE, Mamata H, Nabavi A, Jolesz FA, Kikinis R. Processing and visualization for diffusion tensor MRI. *Medical Image Analysis*. 2002 Jun; vol. 6(no. 2):93–108. [PubMed: 12044998]
26. Susil RC, Krieger A, Derbyshire JA, Tanacs A, Whitcomb LL, Fichtinger G, Atalar E. System for MR image-guided prostate interventions: Canine study. *Radiology*. 2003 Sep; vol. 228(no. 3):886–894. [PubMed: 12954903]

27. Chowning SL, Susil RC, Krieger A, Fichtinger G, Whitcomb LL, Atalar E. A preliminary analysis and model of prostate injection distributions. *Prostate*. 2006 Mar; vol. 66(no. 4):344–357. [Online]. Available: <http://dx.doi.org/10.1002/pros.20298>. [PubMed: 16302267]
28. D'Amico AV, Cormack R, Tempany CM, Kumar S, Topulos G, Kooy HM, Coleman CN. Real-time magnetic resonance image-guided interstitial brachytherapy in the treatment of select patients with clinically localized prostate cancer. *International Journal of Radiation Oncology Biology Physics*. 1998 Oct; vol. 42(no. 3):507–515.
29. Chen JC, Moriarty JA, Derbyshire JA, Peters RD, Trachtenberg J, Bell SD, Doyle J, Arrelano R, Wright GA, Henkelman RM, Hinks RS, Lok SY, Toi A, Kucharczyk W. Prostate cancer: MR imaging and thermometry during microwave thermal ablation-initial experience. *Radiology*. 2000 Jan; vol. 214(no. 1):290–297. [PubMed: 10644139]
30. Graham SJ, Stanisz GJ, Kecojevic A, Bronskill MJ, Henkelman RM. Analysis of changes in MR properties of tissues after heat treatment. *Magnetic Resonance in Medicine*. 1999 Dec; vol. 42(no. 6):1061–1071. [PubMed: 10571927]
31. Tsekos NV, Khanicheh A, Christoforou E, Mavroidis C. Magnetic resonance-compatible robotic and mechatronics systems for image-guided interventions and rehabilitation: a review study. *Annual Review of Biomedical Engineering*. 2007; vol. 9:351–387. [Online]. Available: <http://dx.doi.org/10.1146/annurev.bioeng.9.121806.160642>.
32. Gassert R, Burdet E, Chinzei K. Opportunities and challenges in MR-compatible robotics. *IEEE Engineering in Medicine and Biology Magazine*. 2008 May-Jun; vol. 27(no. 3):15–22. [PubMed: 18519177]
33. Patriciu, A.; Muntener, M.; Kavossi, L.; Stoianovici, D. Image-guided robotic assisted interventions. In: de la Rosette, JJ.; Manyak, MJ.; Harisinghani, MG.; Wijkstra, H., editors. *Imaging in Oncological Urology*. London: Springer; 2009. p. 365-371.
34. Susil R, Krieger A, Derbyshire J, Tanacs A, Whitcomb L, Fichtinger G, Atalar E. A system for guidance and monitoring of transrectal prostate biopsy in a 1.5 T closed MR scanner. *European Radiology*. 2002; vol. 12(9)
35. Krieger, A.; Susil, R.; Tanacs, A.; Fichtinger, G.; Whitcomb, L.; Atalar, E. A mri compatible device for MRI guided transrectal prostate biopsy; *International Society of Magnetic Resonance Imaging in Medicine, Tenth Scientific Meeting*; Honolulu. 2002. p. 338
36. Krieger A, Susil RC, Ménard C, Coleman JA, Fichtinger G, Atalar E, Whitcomb LL. Design of a novel MRI compatible manipulator for image guided prostate interventions. *IEEE Transactions on Biomedical Engineering*. 2005 Feb. vol. 52(no. 2):306–313. [PubMed: 15709668]
37. Ménard C, Susil RC, Choyke P, Coleman J, Grubb R, Gharib A, Krieger A, Guion P, Thomasson D, Ullman K, Gupta S, Espina V, Liotta L, Petricoin E, Fichtinger G, Whitcomb LL, Atalar E, Norman Coleman C, Camphausen K. An interventional magnetic resonance imaging technique for the molecular characterization of intraprostatic dynamic contrast enhancement. *Molecular Imaging*. 2005; vol. 4(no. 1):63–66.
38. Susil RC, Ménard C, Krieger A, Coleman JA, Camphausen K, Choyke P, Fichtinger G, Whitcomb LL, Coleman CN, Atalar E. Transrectal prostate biopsy and fiducial marker placement in a standard 1.5 T magnetic resonance imaging scanner. *Journal of Urology*. 2006 Jan; vol. 175(no. 1):113–120. [Online]. Available: [http://dx.doi.org/10.1016/S0022-5347\(05\)00065-0](http://dx.doi.org/10.1016/S0022-5347(05)00065-0). [PubMed: 16406885]
39. Singh AK, Guion P, Sears-Crouse N, Ullman K, Smith S, Albert PS, Fichtinger G, Choyke PL, Xu S, Kruecker J, Wood BJ, Krieger A, Ning H. Simultaneous integrated boost of biopsy proven, MRI defined dominant intra-prostatic lesions to 95 Gray with IMRT: early results of a phase I NCI study. *Radiation Oncology*. 2007; vol. 2:36. [Online]. Available: <http://dx.doi.org/10.1186/1748-717X-2-36>. [PubMed: 17877821]
40. Singh AK, Krieger A, Lattouf J-B, Guion P, Grubb RL, Albert PS, Metzger G, Ullman K, Smith S, Fichtinger G, Ocak I, Choyke P, Ménard C, Coleman J. Patient selection determines the prostate cancer yield of dynamic contrast-enhanced magnetic resonance imaging-guided transrectal biopsies in a closed 3-Tesla scanner. *BJU International*. 2008 Jan; vol. 101(no. 2):181–185. [Online]. Available: <http://dx.doi.org/10.1111/j.1464-410X.2007.07219.x>. [PubMed: 17922874]
41. Krieger, A.; Guion, P.; Csoma, C.; Iordachita, I.; Singh, AK.; Kaushal, A.; Fichtinger, G.; Whitcomb, LL. Design and preliminary clinical studies of an MRI-guided transrectal prostate

- intervention system. Seventh Interventional MRI Symposium; September 12 and 13, 2008; Baltimore, Maryland. 2008. on
42. Krieger, A.; Metzger, G.; Fichtinger, G.; Atalar, E.; Whitcomb, LL. A hybrid method for 6-DOF tracking of MRI-compatible robotic interventional devices. Proceedings - IEEE International Conference on Robotics and Automation; May 2006; Orlando, FL, United States. 2006. p. 3844-3849.
 43. Beyersdorff D, Winkel A, Hamm B, Lenk S, Loening SA, Taupitz M. MR imaging-guided prostate biopsy with a closed MR unit at 1.5 T: Initial results. *Radiology*. 2005 Feb; vol. 234(no. 2):576–581. [PubMed: 15616117]
 44. Engelhard K, Hollenbach HP, Kiefer B, Winkel A, Goeb K, Engehausen D. Prostate biopsy in the supine position in a standard 1.5-T scanner under real time MR-imaging control using a MR-compatible endorectal biopsy device. *European Radiology*. 2006 Jun; vol. 16(no. 6):1237–1243. [Online]. Available: <http://dx.doi.org/10.1007/s00330-005-0100-6>. [PubMed: 16447048]
 45. Futterer, J.; Schouten, M.; Scheenen, T.; Barentsz, J. MR-compatible transrectal prostate biopsy robot: A feasibility study. 16th Annual ISMRM Scientific Meeting and Exhibition; ISMRM; 2010.
 46. Elhawary H, Zivanovic A, Rea M, Davies B, Besant C, McRobbie D, de Souza N, Young I, Lamperth M. The feasibility of MR-image guided prostate biopsy using piezoceramic motors inside or near to the magnet isocentre. *International Conference on Medical Image Computing and Computer-Assisted Intervention*. 2006; vol. 9(no. Pt 1):519–526.
 47. D'Amico AV, Tempny CM, Cormack R, Hata N, Jinzaki M, Tuncali K, Weinstein M, Richie JP. Transperineal magnetic resonance image guided prostate biopsy. *Journal of Urology*. 2000 Aug; vol. 164(no. 2):385–387.
 48. Susil RC, Camphausen K, Choyke P, McVeigh ER, Gustafson GS, Ning H, Miller RW, Atalar E, Coleman CN, Ménard C. System for prostate brachytherapy and biopsy in a standard 1.5 T MRI scanner. *Magnetic Resonance in Medicine*. 2004 Sep; vol. 52(no. 3):683–687. [PubMed: 15334592]
 49. Chinzei K, Hata N, Jolesz FA, Kikinis R. MRI compatible surgical assist robot: System integration and preliminary feasibility study. *Medical Image Computing and Computer-Assisted Intervention (MICCAI)*. 2000 Oct.vol. 1935:921–930.
 50. DiMaio SP, Pieper S, Chinzei K, Hata N, Haker SJ, Kacher DF, Fichtinger G, Tempny CM, Kikinis R. Robot-assisted needle placement in open MRI: system architecture, integration and validation. *Comput Aided Surgery*. 2007 Jan; vol. 12(no. 1):15–24. [Online]. Available: <http://dx.doi.org/10.1080/10929080601168254>.
 51. Tadakuma, K.; DeVita, L.; Y, S.; Dubowsky, S. The experimental study of a precision parallel manipulator with binary actuation: With application to MRI cancer treatment. *Proc. IEEE International Conference on Robotics and Automation ICRA '08*; 2008 May-May. p. 2503-2508.
 52. Plante, J.; Devita, L.; Tadakuma, K.; Dubowsky, S. MRI Compatible Device for Robotic Assisted Interventions to Prostate Cancer, in *Biomedical Applications of Electroactive Polymer Actuators*. John Wiley and Sons; 2009. ch. 22.
 53. Stoianovici D, Song D, Petrisor D, Ursu D, Mazilu D, Muntener M, Mutener M, Schar M, Patriciu A. MRI stealth robot for prostate interventions. *Minimally Invasive Therapy and Allied Technologies*. 2007; vol. 16(no. 4):241–248. [Online]. Available: <http://dx.doi.org/10.1080/13645700701520735>. [PubMed: 17763098]
 54. Fischer GS, Iordachita I, Csoma C, Tokuda J, DiMaio SP, Tempny CM, Hata N, Fichtinger G. MRI-compatible pneumatic robot for transperineal prostate needle placement. *IEEE/ASME Transactions on Mechatronics*. 2008 Jun; vol. 13(no. 3):295–305. [PubMed: 21057608]
 55. Song, S-E.; Cho, NB.; Fischer, G.; Hata, N.; Tempny, C.; Fichtinger, G.; Iordachita, I. Development of a pneumatic robot for MRI-guided transperineal prostate biopsy and brachytherapy: New approaches. *Proc. IEEE Int Robotics and Automation (ICRA) Conf*; 2010. p. 2580-2585.
 56. Goldenberg AA, Trachtenberg J, Kucharczyk W, Yi Y, Haider M, Ma L, Weersink R, Raoufi C. Robotic system for closed-bore MRI-guided prostatic interventions. *IEEE/ASME Transactions on Mechatronics*. 2008 Jun.vol. 13(no. 3):374–379.

57. van den Bosch MR, Moman MR, van Vulpen M, Battermann JJ, Duiveman E, van Schelven LJ, de Leeuw H, Lagendijk JJW, Moerland MA. MRI-guided robotic system for transperineal prostate interventions: proof of principle. *Phys Med Biol*. 2010 Mar; vol. 55(no. 5):N133–N140. [Online]. Available: <http://dx.doi.org/10.1088/0031-9155/55/5/N02>. [PubMed: 20145293]
58. Zangos S, Eichler K, Engelmann K, Ahmed M, Dettmer S, Herzog C, Pegios W, Wetter A, Lehnert T, Mack MG, Vogl TJ. MR-guided transgluteal biopsies with an open low-field system in patients with clinically suspected prostate cancer: technique and preliminary results. *European Radiology*. 2005 Jan; vol. 15(no. 1):174–182. [Online]. Available: <http://dx.doi.org/10.1007/s00330-004-2458-2>. [PubMed: 15351902]
59. Zangos S, Herzog C, Eichler K, Hammerstingl R, Lukoschek A, Guthmann S, Gutmann B, Schoepf UJ, Costello P, Vogl TJ. MR-compatible assistance system for puncture in a high-field system: device and feasibility of transgluteal biopsies of the prostate gland. *European Radiology*. 2007 Apr; vol. 17(no. 4):1118–1124. [Online]. Available: <http://dx.doi.org/10.1007/s00330-006-0421-0>. [PubMed: 17031454]
60. Vogl T, Mayer H, Zangos S, Selby J, Ackermann H, Mayer F. Prostate Cancer: MR Imaging-guided Galvanotherapy—Technical Development and First Clinical Results I. *Radiology*. 2007; vol. 245(no. 3):895. [PubMed: 18024456]
61. Gleason DF. Classification of prostatic carcinomas. *Cancer Chemotherapy Reports. Part 1*. 1966; vol. 50(no. 3):125. [PubMed: 5948714]
62. McNeal JE, Bostwick DG, Kindrachuk RA, Redwine EA, Freiha FS, Stamey TA. Patterns of progression in prostate cancer. *Lancet*. 1986 Jan; vol. 1(no. 8472):60–63. [PubMed: 2867314]
63. Stamey TA, McNeal JE, Freiha FS, Redwine E. Morphometric and clinical studies on 68 consecutive radical prostatectomies. *Journal of Urology*. 1988 Jun; vol. 139(no. 6):1235–1241. [PubMed: 3373594]
64. Bostwick DG, Graham SD, Napalkov P, Abrahamsson PA, di Sant'agnese PA, Algaba F, Hoisaeter PA, Lee F, Littrup P, Mostofi FK. Staging of early prostate cancer: a proposed tumor volume-based prognostic index. *Urology*. 1993 May; vol. 41(no. 5):403–411. [PubMed: 8488608]
65. Stamey TA, Freiha FS, McNeal JE, Redwine EA, Whittemore AS, Schmid HP. Localized prostate cancer. relationship of tumor volume to clinical significance for treatment of prostate cancer. *Cancer*. 1993 Feb; vol. 71(Suppl)(no. 3):933–938. [PubMed: 7679045]
66. Epstein JI, Chan DW, Sokoll LJ, Walsh PC, Cox JL, Rittenhouse H, Wolfert R, Carter HB. Nonpalpable stage T1c prostate cancer: prediction of insignificant disease using free/total prostate specific antigen levels and needle biopsy findings. *Journal of Urology*. 1998 Dec; vol. 160(no. 6 Pt 2):2407–2411. [PubMed: 9817393]
67. Goto Y, Ohori M, Arakawa A, Kattan MW, Wheeler TM, Scardino PT. Distinguishing clinically important from unimportant prostate cancers before treatment: value of systematic biopsies. *Journal of Urology*. 1996 Sep; vol. 156(no. 3):1059–1063. [PubMed: 8709307]
68. Nakashima J, Tanimoto A, Imai Y, Mukai M, Horiguchi Y, Nakagawa K, Oya M, Ohigashi T, Marumo K, Murai M. Endorectal MRI for prediction of tumor site, tumor size, and local extension of prostate cancer. *Urology*. 2004 Jul; vol. 64(no. 1):101–105. [Online]. Available: <http://dx.doi.org/10.1016/j.urology.2004.02.036>. [PubMed: 15245944]
69. Fischer, GS.; Krieger, A.; Iordachita, II.; Csoma, C.; Whitcomb, LL.; Fichtinger, G. MRI compatibility of robot actuation techniques – a comparative study; International Conference on Medical Image Computing and Computer-Assisted Intervention; 2008 Sept..
70. Woodson, WE.; Tillman, B.; Tillman, P. Human Factors Design Handbook. McGraw-Hill; 1992.
71. Krieger A, Csoma C, Iordachita II, Guion P, Singh AK, Fichtinger G, Whitcomb LL. Design and preliminary accuracy studies of an mri-guided transrectal prostate intervention system. International Conference on Medical Image Computing and Computer-Assisted Intervention. 2007; vol. 10(no. Pt 2):59–67.
72. Xu, H.; Lasso, A.; Vikal, S.; Guion, P.; Krieger, A.; Kaushal, A.; Whitcomb, LL.; Fichtinger, G. Medical Imaging 2010: Visualization, Image- Guided Procedures, and Modeling. SPIE. San Diego, California, USA: SPIE; 2010. Accuracy validation for MRI-guided robotic prostate biopsy; p. 762 517p. 762 517-762 518.

73. DiMaio SP, Kacher DF, Ellis RE, Fichtinger G, Hata N, Zientara GP, Panych LP, Kikinis R, Jolesz FA. Needle artifact localization in 3T MR images. *Studies in Health Technology and Informatics*. 2006; vol. 119:120–125. [PubMed: 16404029]
74. NEMA. Determination of Signal-to-Noise Ratio (SNR) in Diagnostic Magnetic Resonance Imaging, NEMA Standard Publication MS 1-2008. The Association of Electrical and Medical Imaging Equipment Manufacturers; 2008. <http://www.nema.org/stds/ms1.cfm>
75. Wang, Y.; Cole, G.; Su, H.; Pilitsis, J.; Fischer, G. MRI compatibility evaluation of a piezoelectric actuator system for a neural interventional robot. *Engineering in Medicine and Biology Society*, 2009. EMBC 2009; Annual International Conference of the IEEE; IEEE; 2009. p. 6072-6075.

Biographies



Axel Krieger (M'05) received his Ph.D. in mechanical engineering from the Johns Hopkins University in 2008. Currently he is Product Leader, Prostate Solutions at Sentinelle Medical in Toronto, Canada, a Hologic Division. His research interest focuses on the development of MRI compatible coils and devices for MRI-guided interventions. He has been a member of IEEE since 2005.



Sang-Eun Song (M'10) received a M.Sc. degree in Mechanical Systems Engineering from the University of Liverpool in 2000, and a Ph.D. degree in Mechanical Engineering (Medical Robotics) from Imperial College London, U.K. in 2005. He was a Research Scientist at the Laboratory for Computational Sensing and Robotics, Johns Hopkins University, Baltimore, MD. Currently he is a Research Associate at Radiology Department at the Brigham and Women's Hospital and Harvard Medical School, Boston, MA. His research is on the design, control and clinical implementation of surgical robotic systems.



Nathan Bongjoon Cho received his MS degree in Computer Science from the Johns Hopkins University in 2008. He now is the research engineer at the Laboratory for Computational Sensing and Robotics, Johns Hopkins University, Baltimore, MD. His research is in medical robotics and image guided interventions with MRI and CT.



Iulian I. Iordachita (M'08) received the B.Eng. degree in mechanical engineering, the M.Eng. degree in industrial robots, and the Ph.D. degree in mechanical engineering in 1984, 1989, and 1996, respectively, all from the University of Craiova, Craiova, Romania. He is currently an Assistant Research Professor at the Department of Mechanical Engineering and the Laboratory for Computational Sensing and Robotics, Johns Hopkins University, Baltimore, MD, where he is engaged in research on robotics, in particular, robotic hardware. His current research interests include design and manufacturing of surgical instrumentation and devices, medical robots, and mechanisms and mechanical transmissions for robots.



Peter Guion (M'05) received his MS degree in Aerospace Engineering from the University of Maryland, College Park in 2003. He has also earned BS degrees in Mechanical and Electrical Engineering from Virginia Tech (1996) and the University of Maryland, College Park (1999), respectively. He is the staff engineer at the Radiation Oncology Branch, National Cancer Institute in Bethesda, MD. His research is in robotics and control systems, with a focus on MRI-guided procedures.



Gabor Fichtinger (M'04) received a Ph.D. degree in computer science from the Technical University of Budapest, Hungary in 1990. He is Professor in the School of Computing, with cross appointments in the Departments of Mechanical and Material Engineering, Electrical and Computer Engineering, and Surgery, at Queen's University, Kingston, Canada, where he directs the Percutaneous Surgery Laboratory. His research specializes on system development for computer-assisted interventions, with special focus on image-guided oncology applications. He holds a Level-1 Cancer Care Ontario Research Chair in Cancer Imaging.



Louis L. Whitcomb (S'86-M'95-SM'02-F'11) received a Ph.D. degree in electrical engineering from Yale University 1992. He is Professor in the Department of Mechanical Engineering, with secondary appointment in the Department of Computer Science, Johns Hopkins University, Baltimore, MD, USA, where he directs JHU's Laboratory for

Computational Sensing and Robotics. His research is on the design, dynamics, and control of robotic systems, with focus on image guided systems for intervention in extreme environments, with focus on MRI-guided international systems. He is the Louis R. Sardella Faculty Scholar and a Fellow of the IEEE.

\$watermark-text

\$watermark-text

\$watermark-text

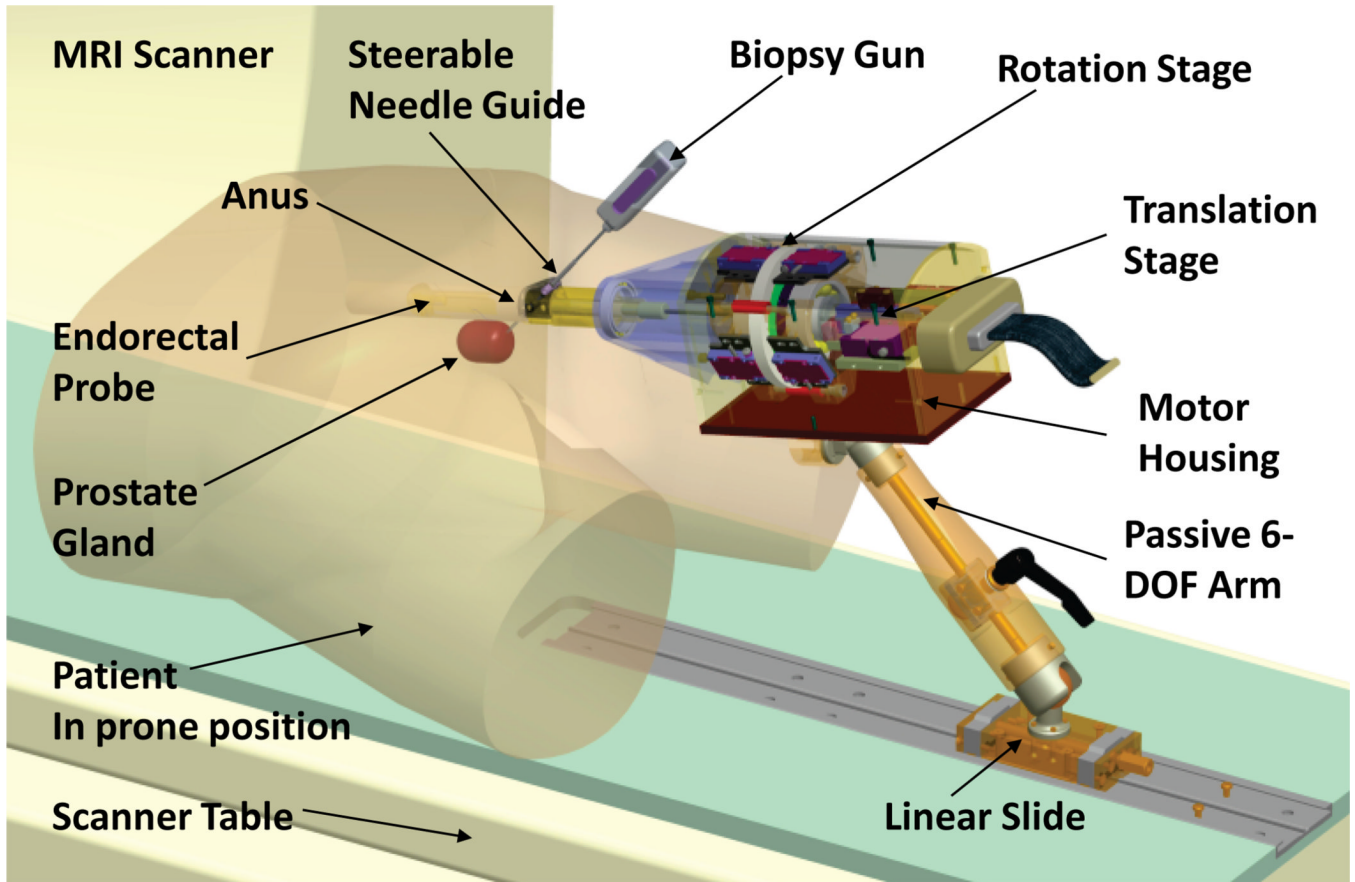


Fig. 1. CAD model of the APT-III actuated robot for prostate intervention, showing the actuated robot (motor housing, translation stage, rotation stage, steerable needle guide, and endorectal probe with of steerable needle guide and integral MR antenna.) The robot is carried on a passive positioning arm attached to a linear slide on the MR scanner table. Biopsy gun and outline of prostate are shown, indicating prone positioning in a transrectal prostate biopsy procedure. The APT-III employs the rectal probe, steerable needle guide, and passive arm designed originally for the APT-II; all other parts are newly designed specifically for the APT-III.

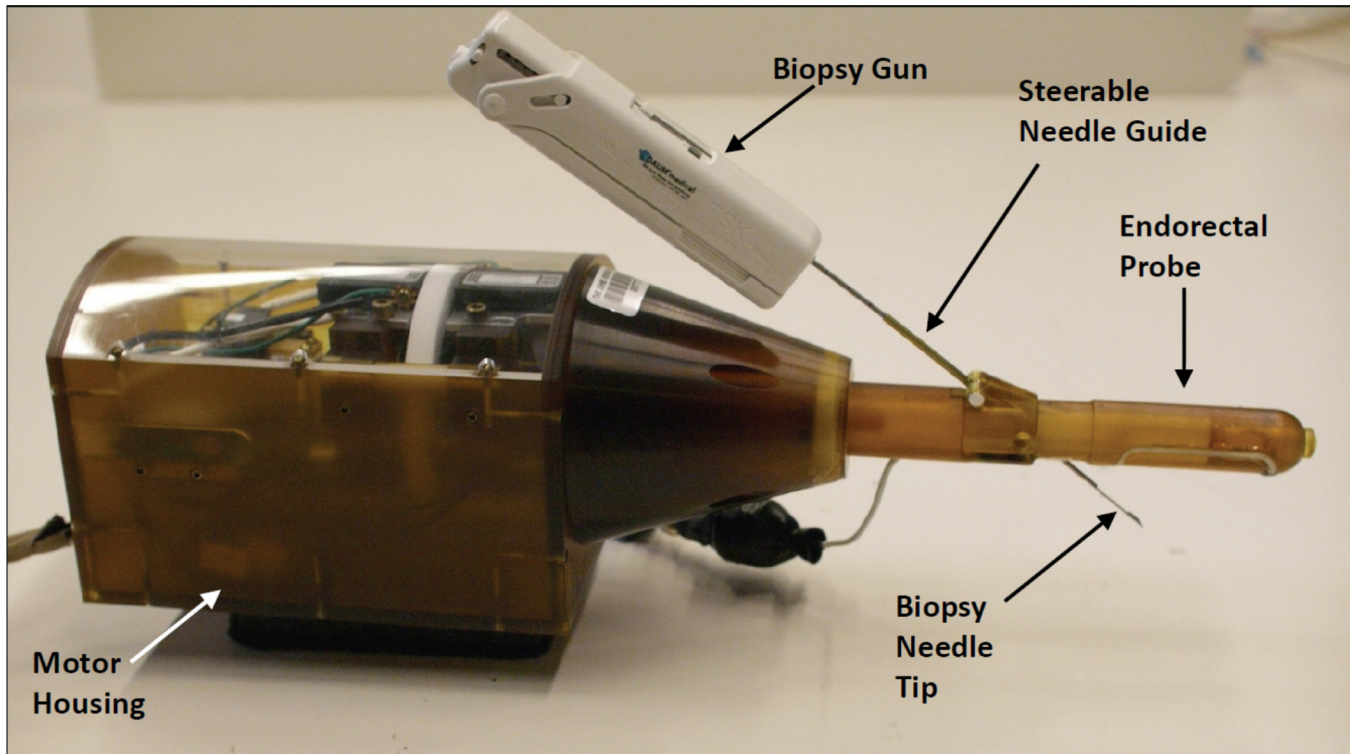


Fig. 2. Close-up photograph of the APT-III actuated robot for prostate intervention with an automatic biopsy needle inserted in needle guide.

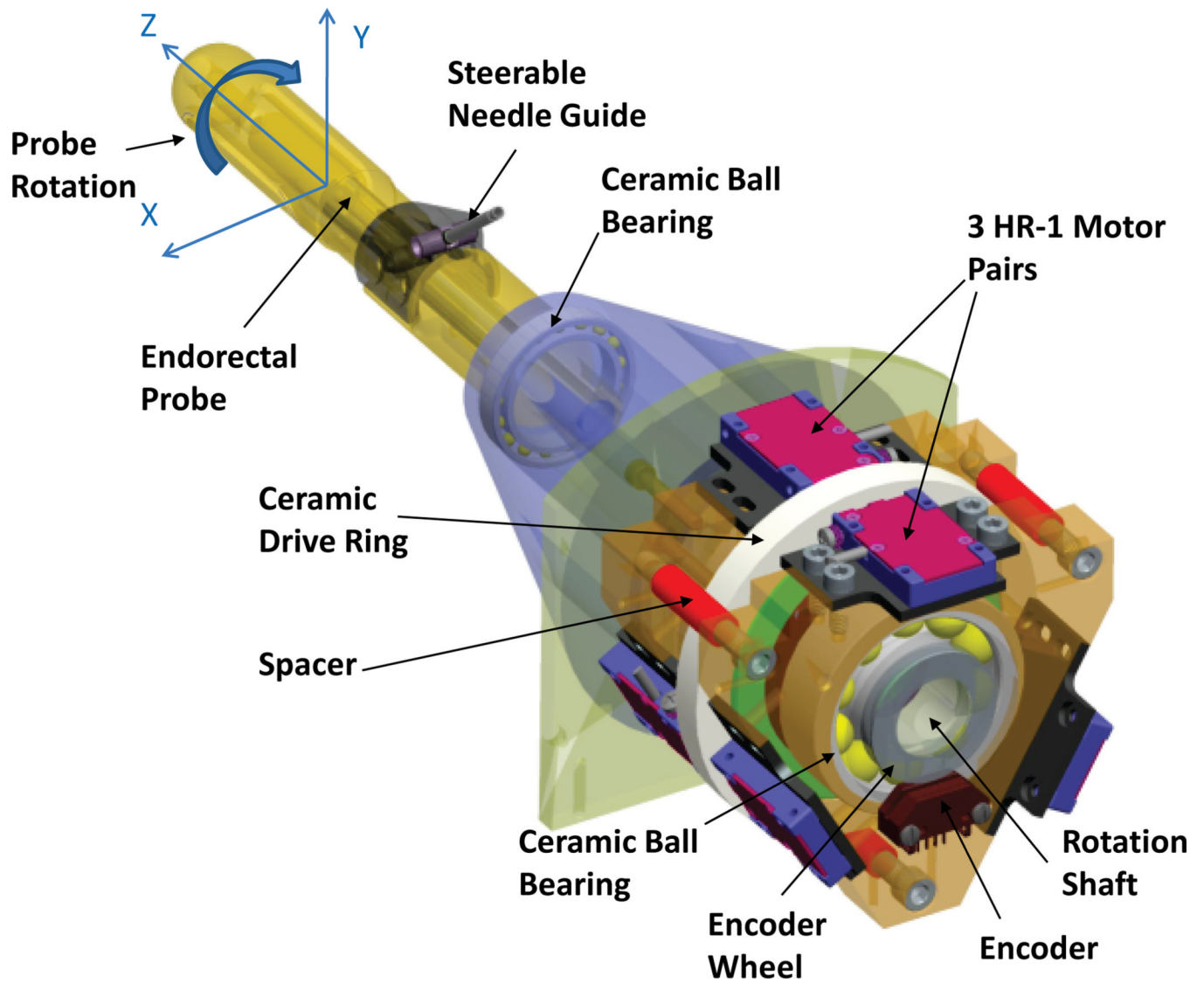


Fig. 3. CAD model of the rotation stage for the actuated robot. Three pairs of HR-1 Nanomotion motors rotate a ceramic ring placed on the rotation shaft.

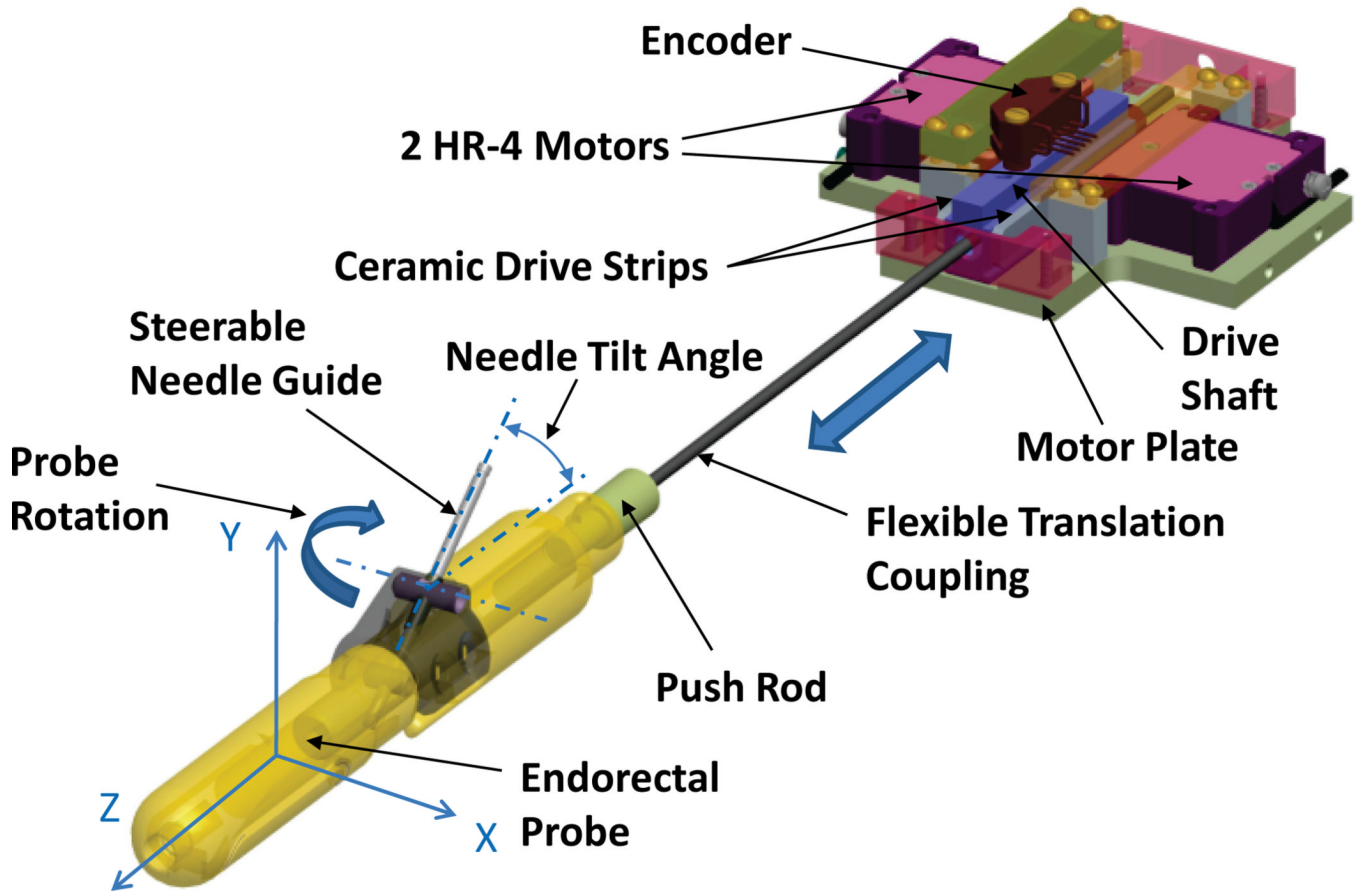


Fig. 4. CAD model of the translation stage for the actuated robot. The translation stage controls the tilt angle of the steerable needle guide within the transrectal probe. A pair of HR-4 Nanomotion motors pushes on ceramic drive strips and provides linear motion of a drive shaft.

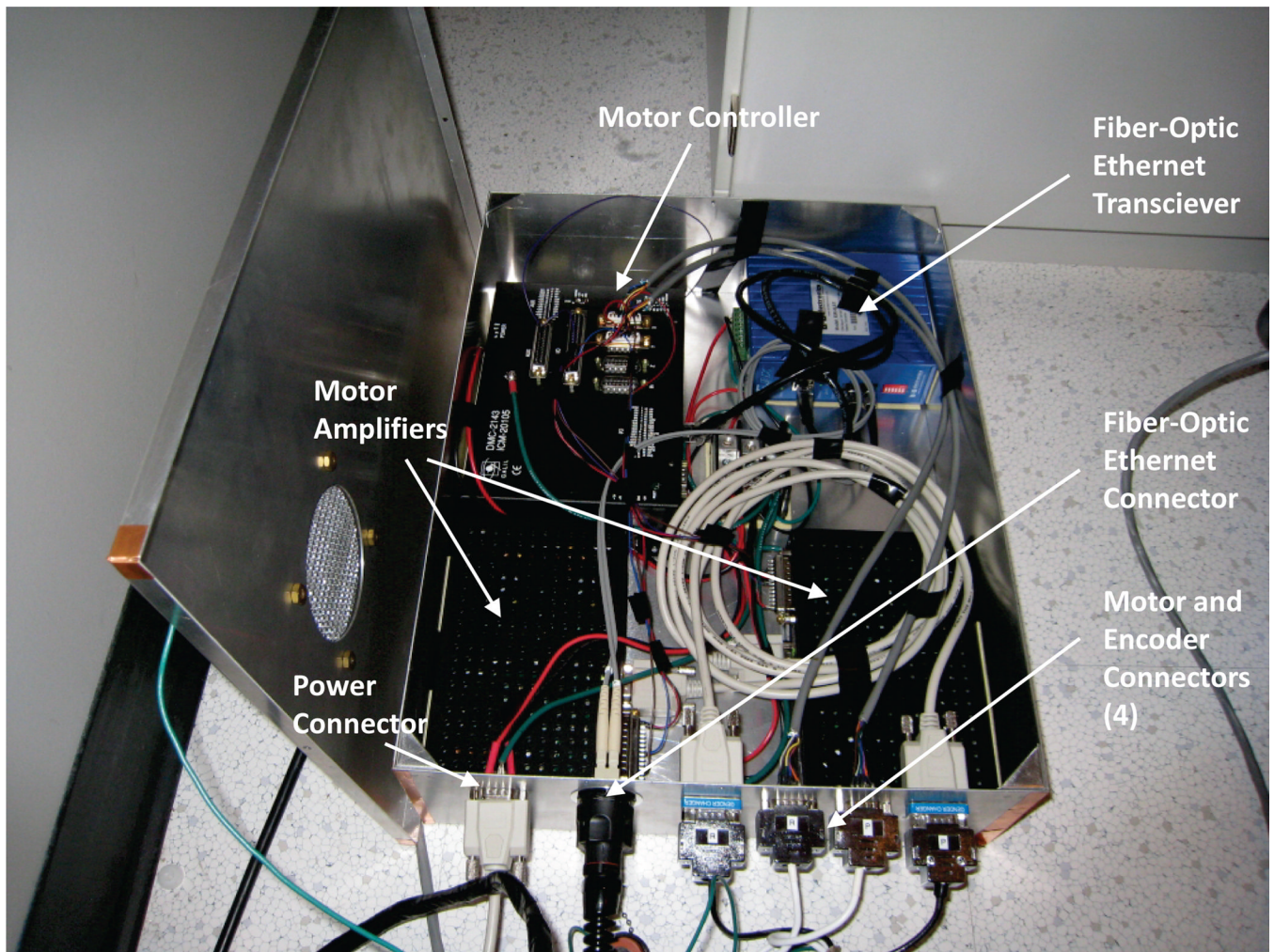


Fig. 5. Photograph of the controller box designed to be placed inside the MRI scanner room near the control room wall waveguide that allows passage of electrical and fiber-optic cables. The box contains motor amplifiers, motion controller, and Ethernet media converter.

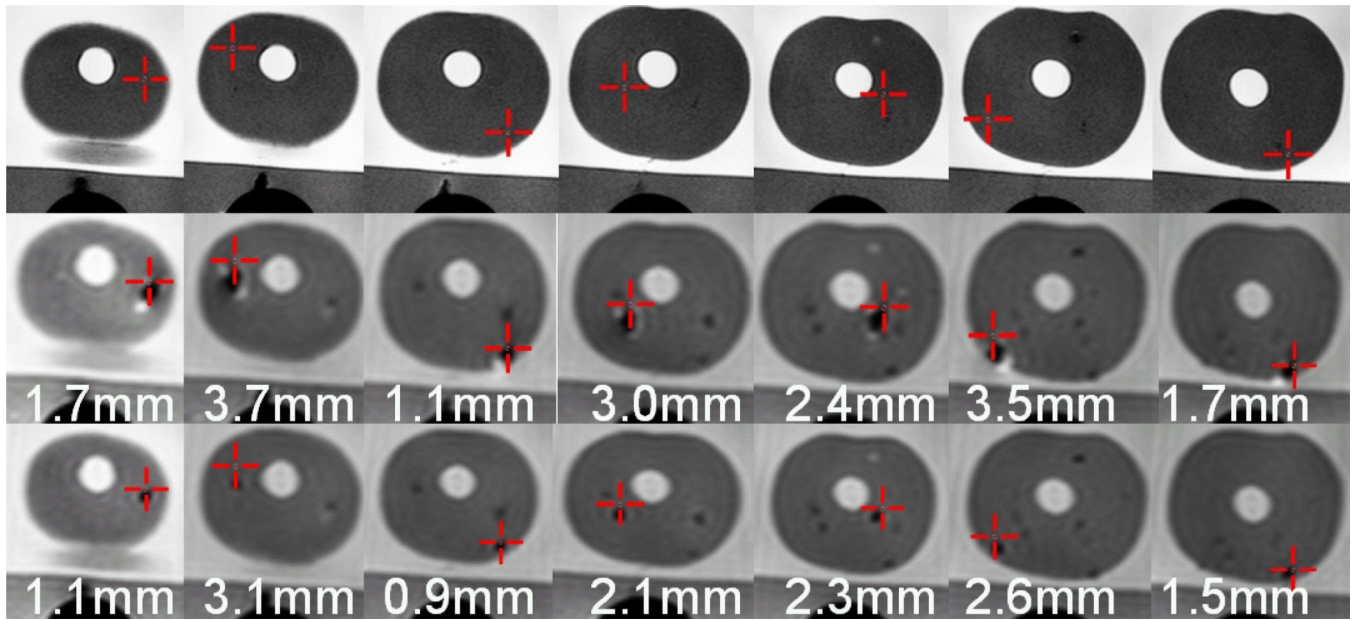


Fig. 6.

Targeting images, biopsy needle confirmation images, glass needle confirmation images and in-plane errors for seven biopsies of a prostate phantom using the actuated transrectal prostate robot. First row: A target (cross hairs) is selected on axial TSE T2 weighted images. Second row: The biopsy needle tip void is visualized in an axial TSE proton density image. The desired target approximately matches the actual position of the needle. Third row: The glass needle tip void is visualized in an axial TSE proton density image. The void for the glass needle is much smaller than for the biopsy needle and closer to the selected target. Numbers indicate the in-plane needle targeting error for the needle placement.

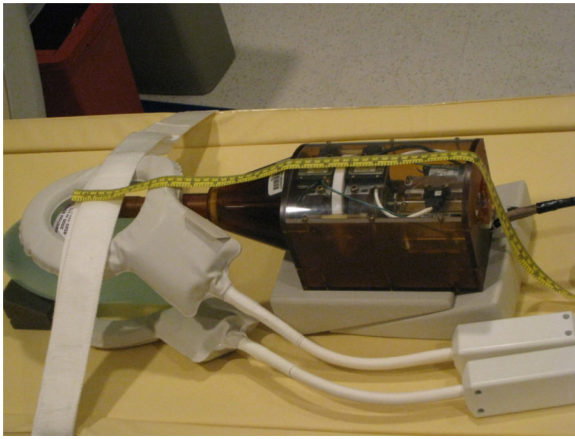


Fig. 7. Experimental setup for SNR tests in a 3 T MRI scanner. Left image shows unshielded robot, saline phantom, and imaging coils. Right image shows the robot with the addition of radio-frequency (RF) shielding.

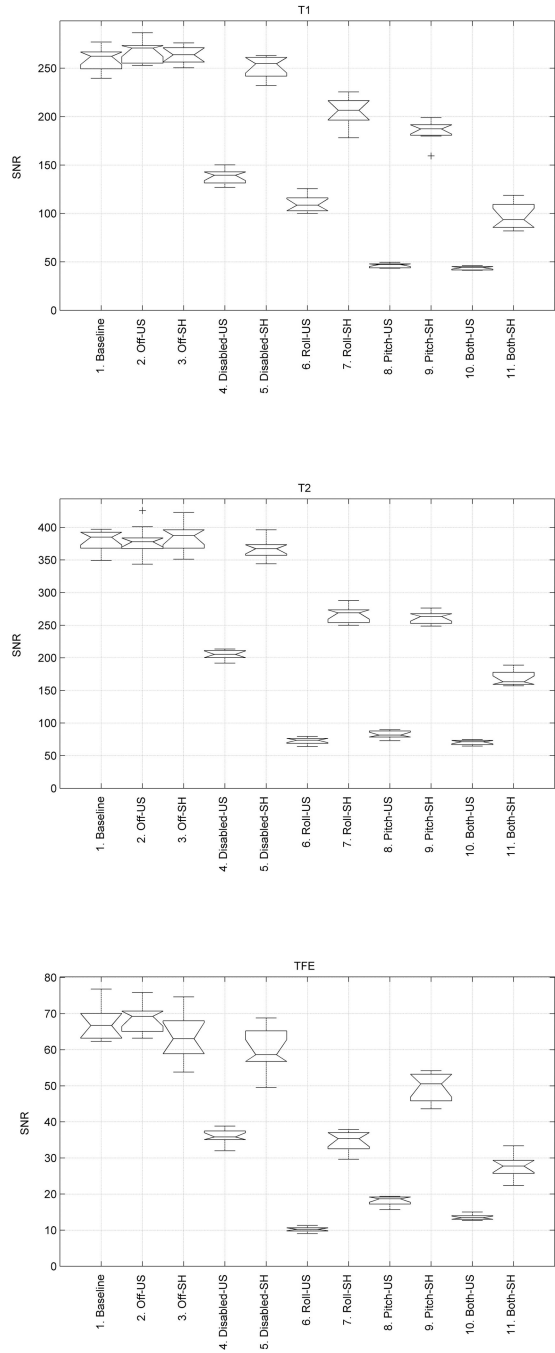


Fig. 8. MRI Signal-to-Noise Ratio (SNR) for T1 scans (top), T2 scans (middle), and TFE scans (bottom). T1, T2, and TFE MRI scan parameters are given in Table I. Eleven different robot test configurations (labeled 1–11) are given in Table II.

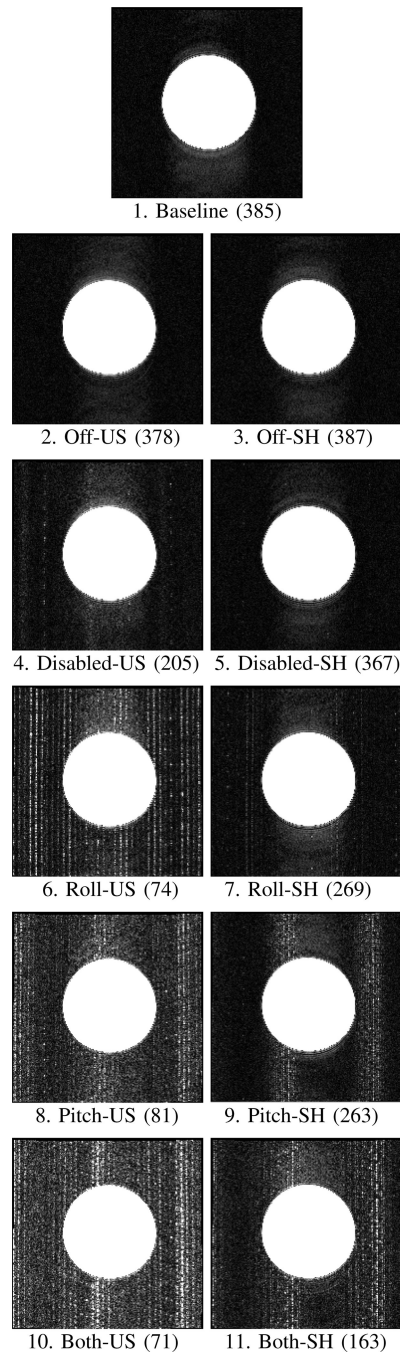


Fig. 9. Representative T2 phantom images from the SNR tests showing (from top to bottom) 1. Baseline; 2,3: Off; 4,5: Disabled; 6,7: Roll; 8,9: Pitch; and 10,11: Both. Left images are for the case of the unshielded robot. Right images are for the case of the shielded robot. T2 MRI scan parameters are given in Table I. Eleven different robot test configurations (labeled 1–11) are given in Table II. SNR values are given in parenthesis for each scan.

TABLE I

MRI scan parameters for motor compatibility trial.

Scan	Slice mm	FOV mm	Slices	TE ms	TR ms	Flip Angle deg	NEX	Pixel band- width Hz pixel
T1	5	240	3	2.3	225	75°	1	1059.0
T2	5	240	3	90	3000	90°	1	1035.7
TFE	5	240	3	10	26	70°	1	1752.5

TABLE II

Eleven robot test configurations for SNR test.

LABEL	TEST CONDITION
1. Baseline:	Image the phantom with no robot or controller present in the scanner room.
2. Off-US:	Image the phantom after placing the robot next to the phantom and the transrectal probe on top of the phantom. The phantom and sheath position approximate prostate and sheath position in a clinical procedure. The controller is located in the scanner room, connected, but powered off.
3. Off-SH:	As per (2), with additional shielding on robot.
4. Disab-US:	Image the phantom after powering on the controller, but disabling the motor amplifiers.
5. Disab-SH:	As per (4), with additional shielding on the robot.
6. Roll-US:	Image the phantom with the roll motor amplifier enabled, but the motor not moving.
7. Roll-SH:	As per (6), with additional shielding on the robot.
8. Pitch-US:	Image the phantom with the pitch (translation) motor amplifier enabled.
9. Pitch-SH:	As per (8), with additional shielding on the robot.
10. Both-US:	Image the phantom with both roll and pitch (translation) motor amplifiers enabled.
11. Both-SH:	As per (10), with additional shielding on robot.